Neurobiology of Disease 95 (2016) 35–45

Contents lists available at ScienceDirect

Neurobiology of Disease

journal homepage: www.elsevier.com/locate/ynbdi

In vivo imaging reveals impaired connectivity across cortical and subcortical networks in a mouse model of DYT1 dystonia

Jesse C. DeSimone [a], Marcelo Febo [b], Priyank Shukla [a], Edward Ofori [a], Luis M. Colon-Perez [b], Yuqing Li [c], David E. Vaillancourt [a,c,d,*]

[a] Department of Applied Physiology and Kinesiology, University of Florida, Gainesville, FL, USA
[b] Department of Psychiatry, College of Medicine, University of Florida, Gainesville, FL, USA
[c] Department of Neurology, College of Medicine, University of Florida, Gainesville, FL, USA
[d] Department of Biomedical Engineering, University of Florida, Gainesville, FL, USA

ARTICLE INFO

Article history:
Received 2 June 2016
Revised 27 June 2016
Accepted 8 July 2016
Available online 9 July 2016

Keywords:
Diffusion MRI
DYT1 dystonia
Free-water
Functional connectivity
Functional MRI

ABSTRACT

Developing in vivo functional and structural neuroimaging assays in Dyt1 ΔGAG heterozygous knock-in (Dyt1 KI) mice provide insight into the pathophysiology underlying DYT1 dystonia. In the current study, we examined in vivo functional connectivity of large-scale cortical and subcortical networks in Dyt1 KI mice and wild-type (WT) controls using resting-state functional magnetic resonance imaging (MRI) and an independent component analysis. In addition, using diffusion MRI we examined how structural integrity across the basal ganglia and cerebellum directly relates to impairments in functional connectivity. Compared to WT mice, Dyt1 KI mice revealed increased functional connectivity across the striatum, thalamus, and somatosensory cortex; and reduced functional connectivity in the motor and cerebellar cortices. Further, Dyt1 KI mice demonstrated elevated free-water (FW) in the striatum and cerebellum compared to WT mice, and increased FW was correlated with impairments in functional connectivity across basal ganglia, cerebellum, and sensorimotor cortex. The current study provides the first in vivo MRI-based evidence in support of the hypothesis that the deletion of a 3-base pair (ΔGAG) sequence in the Dyt1 gene encoding torsinA has network level effects on in vivo functional connectivity and microstructural integrity across the sensorimotor cortex, basal ganglia, and cerebellum.

1. Introduction

Early-onset generalized torsion dystonia (DYT1) is an autosomal dominant movement disorder with reduced penetrance that typically presents during early childhood through adolescence (Fahn, 1988; Ozelius and Lubarr, 1993). Motor impairments are characterized by involuntary and sustained hyperactive muscle contractions resulting in uncontrolled upper and lower extremity movements and disabling posture (Albanese et al., 2013; Breakefield et al., 2008). In humans, DYT1 represents the most common genetic hallmark of the primary dystonias, and is caused by a trinucleotide (ΔGAG) deletion in one allele of the DYT1 (TOR1A) gene, and corresponding removal of a single glutamic acid residue (ΔE) in the carboxyl terminal region of the torsinA (TA) protein (Breakefield et al., 2008; Ozelius et al., 1997). TA is a member of AAA+ family of ATPases and is associated with a plethora of cellular chaperone functions including the provision of protein folding, neuroprotective refuge of oxidative stress, and prevention of protein aggregate formation (Goodchild and Dauer, 2005; Goodchild et al., 2015; Hewett et al., 2007).

Magnetic resonance imaging (MRI) in Tor1a (Dyt1) ΔGAG heterozygous knock-in (KI) mice (Dang et al., 2005; Goodchild et al., 2005) provides a translational basis for understanding the pathophysiology underlying DYT1 dystonia. In particular, the Dyt1 KI mouse model represents a genetically derived experimental corollary akin to most human DYT1 dystonia patients (Ozelius et al., 1997). As well, although not possessive of an unconcealed spasmodic or contracture-like behavioral phenotype (Breakefield et al., 2008), Dyt1 KI mice exhibit sustained electromyographic (EMG) potential and intermittent co-contractions of opposing muscle groups (DeAndrade et al., 2016), which is a core feature of human patients with dystonia (Berardelli et al., 1998; van der Kamp et al., 1989). Previous work using ^{18}fludeoxyglucose positron emission tomography (PET) in vivo has demonstrated increased regional metabolic activity in the cerebellar vermis of Dyt1 KI mice (Uluğ et al., 2011) and Tor1a heterozygous knock-out (Dyt1 KO) mice (Vo et al., 2015a). Similar regional cerebellar metabolic abnormalities have been evidenced in a Dyt1 transgenic mouse model over-

Abbreviations: DYT1 (TOR1A), human torsinA gene; Dyt1 (Tor1a), mouse torsinA gene; FA_T, free-water corrected fractional anisotropy; FW, free-water; ICA, independent component analysis; KI, knock-in mouse; KO, knock-out mouse; WT, wild-type mouse.

* Corresponding author at: Department of Applied Physiology and Kinesiology, University of Florida, P.O. Box 118205, Gainesville 32611-8205, FL, USA.
E-mail address: vcourt@ufl.edu (D.E. Vaillancourt).

Available online on ScienceDirect (www.sciencedirect.com).

http://dx.doi.org/10.1016/j.nbd.2016.07.005
0969-9961/

expressing human mutant TA (so-called hMT mice: Zhao et al., 2011). An interesting question arising from this work is whether impaired functional connectivity exists in the cerebellum and other connected networks such as sensorimotor cortical and basal ganglia regions. The basis for this question stems from previous work employing high-frequency stimulation (HFS) and striatal field potential recordings in vitro showing that Dyt1 KI and hMT mice, elicit an impaired inhibitory modulation and plasticity of cortico-striatal synaptic transmission (i.e., long-term depression: LTD: Dang et al., 2012; Martella et al., 2009; Wang et al., 2006). Moreover, although PET provides a robust measure of glucose utilization, it does not describe how functional networks are temporally correlated and functionally connected (Calhoun et al., 2001a; Calhoun et al., 2001b). Since dystonia has been described as a functional circuit disorder (for reviews see: Berardelli et al., 1998; Breakefield et al., 2008; Tanabe et al., 2009), it is important to determine how a ΔGAG deletion impairs functional connectivity across cortical and subcortical networks. The present study sought to examine functional connectivity in Dyt1 KI mice using high field (11.1 Tesla) resting-state functional magnetic resonance imaging (fMRI) and an independent component analysis (ICA: Calhoun et al., 2001a; Calhoun et al., 2001b; McKeown et al., 1998). We test the hypothesis that the sensorimotor cortex, basal ganglia, and cerebellum have altered functional connectivity patterns in Dyt1 KI compared to wild-type (WT) mice. A secondary goal of the current study was to determine how changes in structural integrity in the basal ganglia and cerebellum relate to functional connectivity. We use in vivo diffusion magnetic resonance imaging (dMRI) and a bi-tensor model to disentangle diffusion properties of water in brain tissue from that of the free-water (FW) measurement in the extracellular space. We test the hypothesis that elevated FW in both basal ganglia and cerebellum regions will directly relate to functional connectivity impairments across basal ganglia, cerebellar, and cortical networks.

2. Materials and methods

2.1. Animals and housing

Twenty adult male ΔGAG heterozygous knock-in mice (Dyt1 KI) and 20 male neurologically intact wild-type (WT) littermate controls (age range: 3–6 mo.) were used in this experiment. Dyt1 KI mice were prepared and genotyped using the PCR protocol as described by Dang et al. (2005). Mice were housed in groups of three in a temperature and humidity controlled environment, maintained on an alternating 12 h. light-dark cycle (i.e., lights off at 18:00 h), and were provided ad libitum food and water access. Animals were acquired and cared for in accordance with the ethical standards set forth by the Guide for the Care and Use of Laboratory Animals (8th edition, 2011) and the American Association for Laboratory Animal Science guidelines. All experimental protocols and procedures were approved and monitored by Institutional Animal Care and Use Committee (IACUC) at the University of Florida.

2.2. MRI preparation and data acquisition

Mice were anesthetized for the duration of the experiment. Isoflurane anesthesia was delivered using compressed air through a Surgivet vaporizer (Dublin, OH, USA) connected to a charcoal trap. Mice were initially induced at 3–4% isoflurane for 1–2 min in an enclosed knock-in chamber. Anesthesia was reduced to 2% for animal setup and 1.0–1.5% for MRI acquisition. Anesthesia was periodically adjusted to accommodate a respiration rate between 40 and 60 breaths per minute. Animals were placed in a prone position on a custom designed plastic mouse bed equipped with a bite bar to immobilize head motion during scanning. An in-house 2.5 × 3.5 cm quadrature surface transmit/receive coil was affixed to the top of the skull and tuned to 470.7 MHz (^{1}H resonance) for B^1 excitation and signal detection (AMRIS Facility, University of Florida, Gainesville, FL, USA). Respiration rate was monitored using a respiration pad placed beneath the abdomen and core body temperature was maintained between 37 and 38 °C using a recirculating waterbed heating system (SA Instruments, Stony Brook, NY).

MRI data were acquired using an 11.1 Tesla Magnex Scientific horizontal magnet (Agilent, Inc., Santa Clara, CA, USA, 205/120HD gradient set with 120 mm inner gradient bore size; maximum gradient strength 600 mT/m and rise time of 130 μs) at the McKnight Brain Institute, University of Florida. MRI preparation and data acquisition were controlled using Agilent Technologies VNMRJ software (Version 3.1). Preparation of the imaging protocol included localized whole brain voxel shimming for magnetic field homogeneity, and acquisition of reference anatomical scans for real-time visual depiction of animal positioning. The ordering of the MRI protocol consisted of one diffusion weighted scan (1 h 30 min), two resting-state functional scans (8 min each), and one reference anatomical T_2-weighted scan (5 min).

Diffusion weighted images were acquired using an 8-shot echo planar imaging (EPI) sequence with the following parameters: repetition time (TR) = 2500 ms, echo time (TE) = 25.88 ms, field of view = 19.2 × 19.2 mm, flip angle = 90°, max b-value = 900 s/mm^2, averages = 3, dummy scans = 2. Geometry was set up as follows: slices = 12, coronal orientation, thickness = 0.75 mm, gap = 0 mm, data matrix = 128 × 128 in-plane.

Functional MRI was performed using a 2-shot EPI sequence with the following parameters: TR = 1000 ms, TE = 20 ms, field of view = 19.2 × 19.2 mm, flip angle = 90°, dummy scans = 4, slices = 12, coronal orientation, thickness = 0.75 mm, gap = 0 mm, data matrix = 64 × 64 in-plane.

Structural images were acquired using a fast-spin echo, T_2-weighted imaging sequence with the following parameters: TR = 2000 ms, field of view = 19.2 × 19.2 mm, slices = 12, coronal orientation, thickness = 0.75 mm, gap = 0 mm, data matrix = 192 × 192 in-plane.

2.3. Functional MRI data processing

Functional MRI data pre-processing was performed using the FMRIB Software Library (FSL: Oxford, UK) and custom-designed Unix shell scripts in AFNI (Cox, 1996). First, we discarded the initial five volumes of both EPI sequences for magnetization equilibrium. The remaining volumes were concatenated into a single EPI image consisting of 205 volumes, and all volumes were realigned to time point 0 of the acquisition. The pre-processing analysis pipeline included manual skull stripping for the removal of non-brain tissue, slice-timing correction, and correction of signal distortions due to eddy currents and/or head motion artifacts. To standardize the data, we co-registered the EPI image of each mouse brain to their respective T_2 image, and then registered the T_2 image of each mouse to that of a single mouse brain. The resultant data matrix was applied to the EPI image via affine transformation with limited degrees of freedom and trilinear interpolation using FLIRT (http://fsl.fmrib.ox.ac.uk/fsl/fslwiki/FLIRT). Additionally, we performed spatial normalization and in-plane smoothing on the EPI image using a Gaussian kernel of FWHM 0.4 mm^2 (*x*-*y* planes) and filtered temporal data using a band pass filter with a cut-off frequency between 0.01 and 0.1 Hz.

Resting-state functional connectivity was examined using an independent component analysis (ICA: Calhoun and Adali, 2012; Calhoun et al., 2001a; Calhoun et al., 2001b; McKeown et al., 1998) and the GIFT toolbox extension in MATLAB (Group ICA of fMRI toolbox: http://www.nitrc.org/projects/gift) with Infomax algorithm. To quantify the maximum number of components, a stability analysis using ICASSO bootstrap mode was used – and this analysis determined that 50 mutually exclusive components be extracted for between-group analyses. Once the ICA component was identified, we performed backward regression for each individual subject between each voxel time series and the identified component time series. The Pearson's correlation

coefficient was then transferred to a z-value for each subject, and the z-value extracted from each voxel provides a standardized measure of the degree of connectivity with the ICA component.

2.4. Diffusion MRI processing

Diffusion MRI pre-processing and free-water (FW) analysis were performed using previously described methods (Ofori et al., 2015a; Ofori et al., 2015b; Planetta et al., 2016). We employed a bi-tensor diffusion analysis pipeline (Pasternak et al., 2009) and the algorithm used in humans was modified for rodents. First, we used the FSL and custom designed UNIX shell scripts in AFNI to correct for signal distortions due to eddy currents and/or head motion artifacts, compensate the diffusion gradients for these rotations, and manual skull stripping for the removal of non-brain tissue. FW and FW-corrected fractional anisotropy (FA_T) maps were calculated from the preprocessed motion and eddy current corrected volumes using custom code written in MATLAB (version R2013a; The MathWorks, Natick, MA). To create the FW map, a minimization procedure was used such that a bi-tensor model (Pasternak et al., 2009) was fit to each voxel to generate the FA_T map. The bi-tensor model predicts the signal attenuation in the presence of FW contamination. The FW component is then eliminated from each voxel to generate the FA_T map. To standardize the data, the resultant FW and FA_T maps were registered to a single mouse brain b0 image by an affine transformation matrix with limited degrees of freedom and trilinear interpolation using FLIRT.

2.5. Statistical analysis

In the resting-state fMRI data, we first performed a one-sample t-test to determine in each group the significant clusters following the backward regression to individual ICA components. This t-test identified significant ICA components in each group, and provided confirmation that the technique was successful. Between-group comparisons were examined by submitting functional connectivity z-scores, FW, and FA_T values to voxel-wise, independent-samples t-tests (i.e., Dyt1 KI versus WT). Within- and between-group differences within a single voxel were thresholded at a voxel-level of $P = 0.005$. Functional and diffusion MRI data were corrected for multiple comparisons using a Monte Carlo simulation. The significance level of the contrasts of interest were set at minimum cluster size of 0.200 mm^3, the equivalent of $P < 0.05$ corrected using the family-wise error rate (FWER). Notably, one Dyt1 KI mouse was excluded from fMRI analyses due to incomplete volume acquisition during scanning and five mice (one Dyt1 KI and four WT) were removed from dMRI analyses due to motion-related signal distortions and issues with partial alignment during data pre-processing. For subjects included in both analyses (18 Dyt1 KI, 16 WT), we computed the relation between FW values and functional connectivity z-scores using Pearson's correlation coefficients. Correlations were performed by combining FW and functional connectivity values across Dyt1 KI and WT mice. *P*-values were adjusted for multiple comparisons at a false discovery rate (FDR) of 0.05 using the Benjamini-Hochberg-Yekutieli method in MATLAB.

In a subsequent analysis, we sought to determine if resting-state functional connectivity differences alone could distinguish between mouse genotypes (i.e., Dyt1 KI and WT). To accomplish that objective, in a training cohort of 24 (12 Dyt1 KI, 12 WT) randomly selected mice we extracted the average z-score values from component clusters where significant between-group effects were detected – and submitted data to a linear kernel support vector machine classification algorithm with 10-fold cross-validation using the library for Support Vector Machines (LIBSVM) (Chang and Lin, 2011). Reliability of the algorithm was evaluated in a testing cohort of 15 mice (seven Dyt1 KI, eight WT).

3. Results

3.1. Resting-state fMRI: identifying components at 50-ICASSO

To delineate specific cortical, basal ganglia, and cerebellar components that displayed significant resting-state functional connectivity, we performed within-subjects t-tests on the resting-state fMRI data separately for Dyt1 KI and WT groups. At 50-ICASSO (see Materials and methods), the results yielded reasonable anatomical decomposition of functional component clusters that were either localized to a specific brain region, or region consisting of adjacent anatomical structures. In both groups, we observed a high degree of functional connectivity in several component clusters within each of the general cortical, basal ganglia, and cerebellar areas. In general, voxels expressing the highest degree of connectivity within each individual component were revealed across two to three slices. To elucidate, Fig. 1 provides an exemplar visual depiction of three separate component clusters that overlap across multiple slices within cortical, basal ganglia, and cerebellar brain structures. In line with previous ICA models in mice (Jonckers et al., 2011; Mechling et al., 2014), our results show unilateral functional connectivity patterns such that component clusters localized to one side of the brain were not revealed in homologous structures in the contralateral hemisphere.

3.2. Resting-state fMRI: between-group differences in functional connectivity

To examine resting-state functional connectivity differences within the 50 identified components, we performed an ICA and compared groups using voxel-wise independent samples t-tests (i.e., 19 Dyt1 KI versus 20 WT). Dyt1 KI mice were associated with significantly increased functional connectivity compared to WT controls in the right striatum (Fig. 2A–B), primary somatosensory cortex (Fig. 2B), thalamus (Fig. 3A–B), and hippocampus (all corrected $P < 0.05$). In turn, compared to WT, Dyt1 KI mice showed decreased functional connectivity patterns in the right primary motor cortex (Fig. 2C) and left cerebellar cortex (Fig. 4A–B) (all corrected $P < 0.05$). To further elucidate between-group functional connectivity differences, Fig. 5 shows subject-by-subject average z-score values for the aforementioned components.

Several aforementioned structures revealed multiple component clusters that were significantly different between groups. In terms of the right striatal component, Dyt1 KI mice showed significantly increased functional connectivity in two separate regions. The majority of temporally correlated voxels within each of these components were localized to the right dorsal striatum (Fig. 2A: Dorsal-1, Fig. 2B: Dorsal-2). For the thalamic component, two separate component clusters in the ventral thalamic area (Fig. 3B: Vthal-1, Fig. 3A: Vthal-2) revealed significantly increased functional connectivity in Dyt1 KI mice. Similarly, Fig. 4 shows that Dyt1 KI mice were associated with significantly decreased functional connectivity in two separate component clusters within the cerebellar paramedian (Fig. 4A: PaL) and anisiform (Fig. 4B: AnL) lobules.

In another analysis, we sought to determine if functional connectivity could accurately classify mouse genotype (Dyt1 KI, WT). To that end, we submitted the mean z-score values from clusters where significant between-group differences were detected to a linear kernel support vector machine algorithm with 10-fold cross validation. We separated the mice into a training dataset for the model using 24 mice (12 Dyt1 KI, 12 WT) and a testing dataset that included 15 mice (seven Dyt1 KI, eight WT). As shown in Table 1, the results of the analysis from the training cohort yielded an area under the curve (AUC) classification accuracy between 0.63 and 1.0. Importantly, three key regions that showed a strong AUC in the training dataset and prediction in the testing cohort were the primary motor cortex, dorsal striatum (Dorsal-1), and cerebellar cortex (anisiform lobule). As indicated in Table 1, other multi-region combinations also yielded high AUC and prediction values.

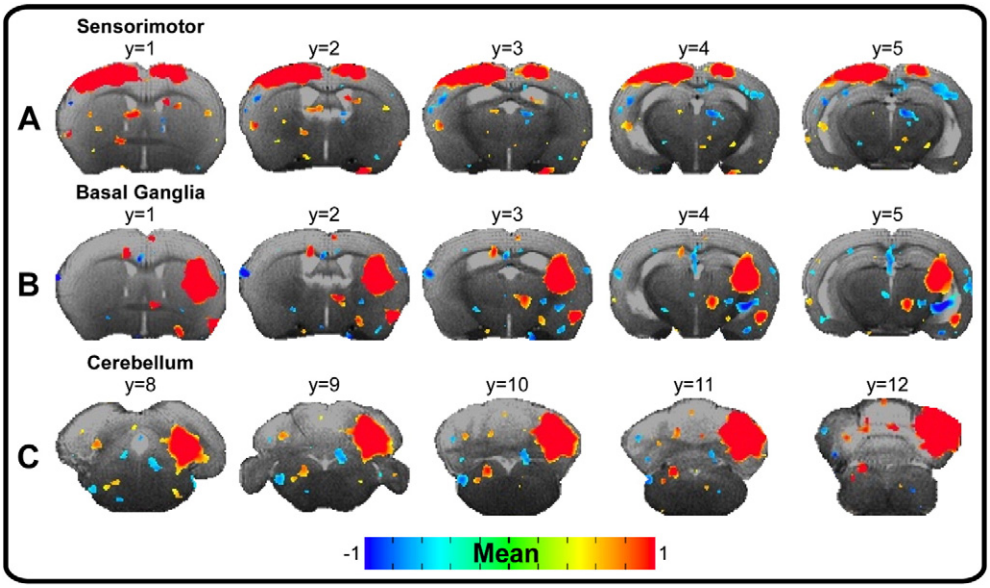

Fig. 1. Exemplar resting-state functional connectivity color maps. Spatial color-coded z-maps of three separate component clusters that overlap across multiple slices in Dyt1 KI mice. Colored voxels provide a measure of mean time-course dependence of resting-state hemodynamic signal fluctuation relative to the mean component time-course. Positive values, represented by warm (red) colors, denote a significant increase in the temporal correlation across voxels within the component, whereas negative values, represented by cold (blue) colors, represent a significant decrease in the temporal correlation across voxels. Results are thresholded at $P < 0.005$ at the voxel level and FWER corrected at $P < 0.05$. (A) Cortical component cluster wherein voxels expressing the highest degree of functional connectivity are localized to the sensorimotor cortex. (B) Basal ganglia component cluster depicting a high degree of functional connectivity localized to the right striatum. (C) Cerebellar component cluster depicting a high degree of functional connectivity within the right cerebellar cortex. Spatial color maps are superimposed over the T_2 weighted image of a single subject.

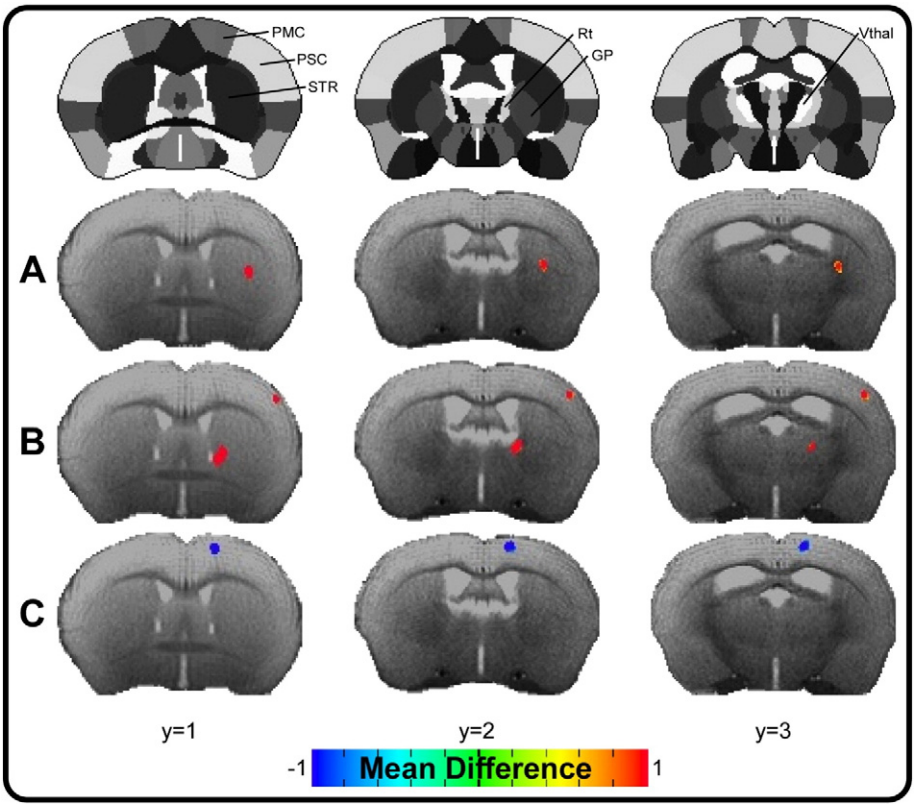

Fig. 2. Between-group cortico-striatal functional connectivity color maps. Color bars represent the mean difference in z-score values for between-group post-hoc comparisons (i.e., Dyt1 KI versus WT). Results are thresholded at $P < 0.005$ at the voxel level and FWER corrected at $P < 0.05$. Positive values, represented by warm (red) colors, denote a significant increase in functional connectivity in Dyt1 KI mice compared to WT mice in the (A-B) dorsal striatum and (B) primary somatosensory cortex, whereas negative values, represented by cold (blue) colors, denote a significant decrease in functional connectivity in Dyt1 KI versus WT mice in the (C) primary motor cortex. Spatial color maps are superimposed over the T_2 weighted image of a single subject. Stereotaxic template atlas provided by Ferris et al. (2014): GP, globus pallidus; PMC, primary motor cortex; PSC, primary somatosensory cortex; Rt, reticular thalamic area; STR, striatum; Vthal, ventral thalamic area.

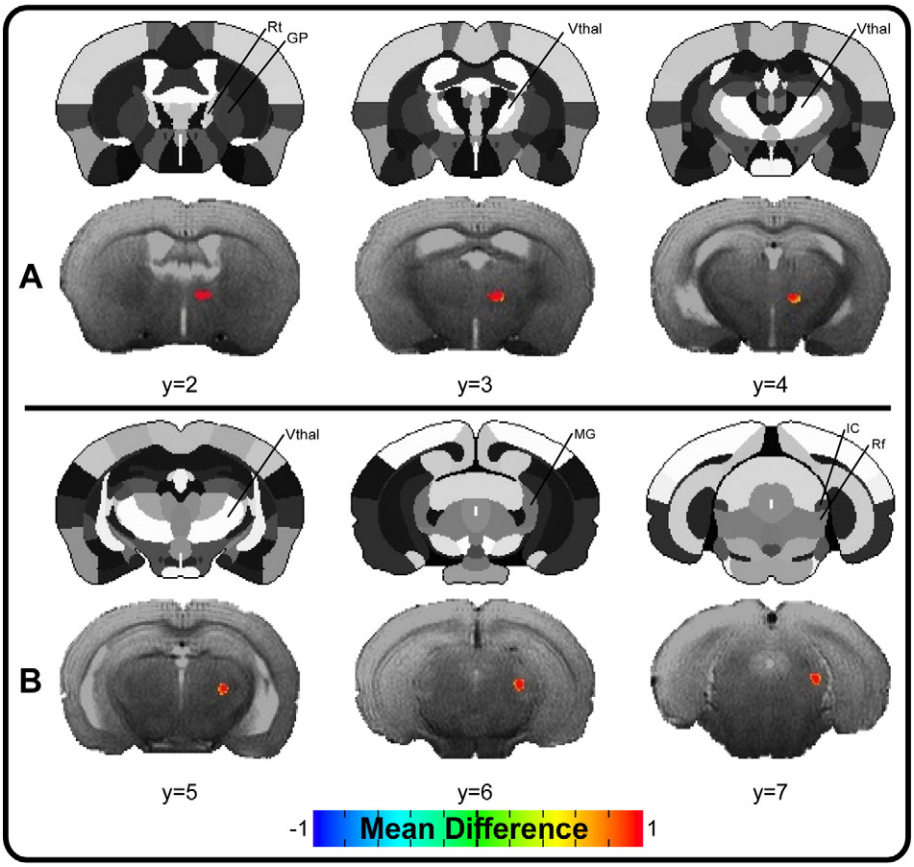

Fig. 3. Between-group thalamic and brainstem functional connectivity color maps. Color bars represent the mean difference in z-score values for between-group post-hoc comparisons (i.e., Dyt1 KI versus WT). Results are thresholded at $P < 0.005$ at the voxel level and FWER corrected at $P < 0.05$. Positive values, represented by warm (red) colors, denote a significant increase in functional connectivity in Dyt1 KI mice compared to WT mice. Dyt1 KI mice demonstrated increased functional connectivity within two thalamic component clusters. The majority of voxels expressing a high degree of connectivity in Dyt1 KI mice were localized to components within the (A–B) ventral thalamic area (A: Vthal-2; B: Vthal-1) and (B) brainstem. Spatial color maps are superimposed over the T_2 weighted image of a single subject. Stereotaxic template atlas provided by Ferris et al. (2014): IC, inferior colliculus; MG, medial geniculate nucleus; Rf, reticular formation; Rt, reticular thalamic area; Vthal, ventral thalamic area.

3.3. Diffusion MRI: free-water and free-water corrected FA

To examine dMRI differences in cortical, basal ganglia, and cerebellar regions between 19 Dyt1 KI and 16 WT mice, we used a bi-tensor analysis model (Pasternak et al., 2009) on the dMRI data and compared FW and FA_T between groups using voxel-wise independent samples t-tests. As shown in Fig. 6, Dyt1 KI mice exhibited increased FW in the right dorsal striatum and lobule II/III of the cerebellum compared to WT controls (all corrected $P < 0.05$). No significant between-group differences in FA_T were detected.

3.4. Correlation analysis

We computed Pearson's correlation coefficients to assess the relation between FW values and functional connectivity in cortical, basal ganglia, and cerebellar regions. We combined subjects' average FW values and functional connectivity z-scores across Dyt1 KI and WT groups. In our first analysis, we computed the relation between FW in the striatum with that of functional connectivity where significant between-group differences were initially detected. As shown in Fig. 7, the results of this analysis yielded a negative correlation between striatal FW and functional connectivity in the paramedian and anisiform lobules of the cerebellum, as well as the primary motor cortex. Our second analysis assessed the relationship between functional connectivity and FW in lobule II/III of the cerebellum. As shown in Fig. 7, cerebellar FW was negatively correlated with functional connectivity in the primary motor cortex and anisiform lobule of the cerebellum. In turn, cerebellar FW and functional connectivity showed a positive correlation in both thalamic regions, striatum (Dorsal-2), and hippocampus.

4. Discussion

The present study provides the first high-field in vivo fMRI- and dMRI-based assays of functional connectivity and structural integrity of cortical, basal ganglia, and cerebellar regions in a mouse model of DYT1 dystonia. It was found that abnormal functional circuit patterns exist across the cortex, basal ganglia, and cerebellum in Dyt1 KI compared with WT mice. Dyt1 KI mice revealed increased functional connectivity across the striatum, thalamus, and somatosensory cortex; and reduced functional connectivity in the motor and cerebellar cortices compared to WT mice. Further, Dyt1 KI mice demonstrated increased FW in the striatum and cerebellum, which directly correlated with changes in functional connectivity.

4.1. Basal ganglia structure-function relationship in Dyt1 KI mice

Previous work has shown that Dyt1 ΔGAG heterozygous KI mice are associated with increased cortico-striatal excitation and LTD deficit (Dang et al., 2012; Yokoi et al., 2015). LTD is thought to underlie plasticity changes related to sensorimotor integration and associative learning of goal-directed movement as more functional synapses are formed between the cortex and striatum (Centonze et al., 2001; Wang et al., 2006). In particular, the level of cortico-striatal activation is modulated by the firing properties of striatal cholinergic interneurons (SCIs)

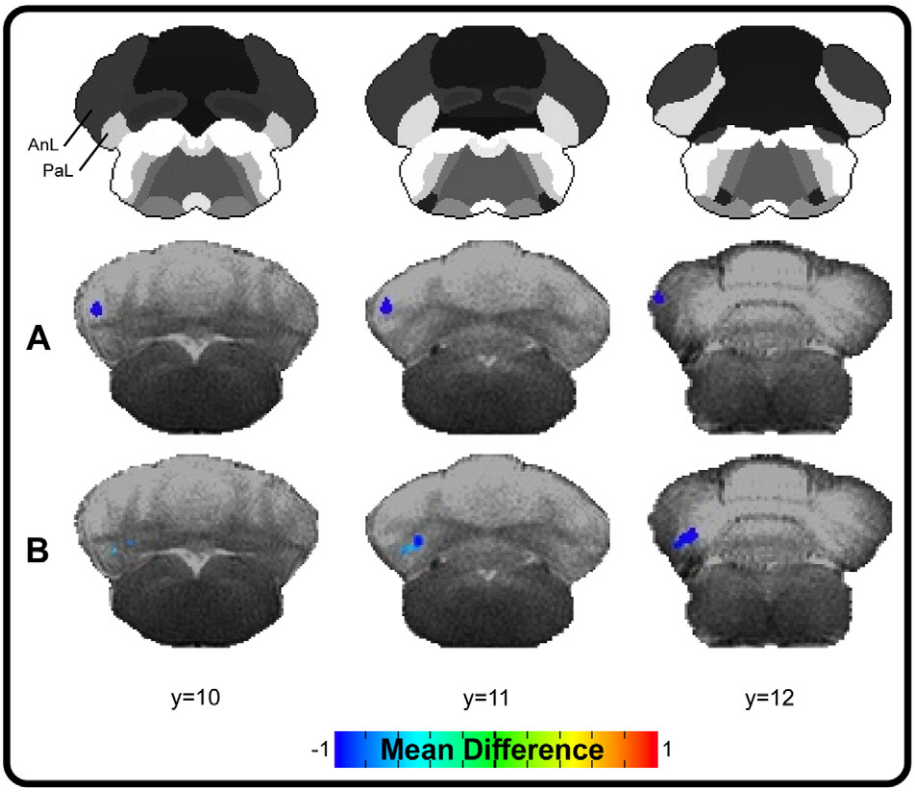

Fig. 4. Between-group cerebellar functional connectivity color maps. Color bars represent mean difference in z-score values for between-group post-hoc comparisons (i.e., Dyt1 KI versus WT). Results are thresholded at $P < 0.005$ at the voxel level and FWER corrected at $P < 0.05$. Negative values, represented by cold (blue) colors, denote a significant decrease in functional connectivity in Dyt1 KI versus WT mice in the (A) paramedian, PaL, and (B) anisiform, AnL, lobules. Spatial color maps are superimposed over the T_2 weighted image of a single subject. Stereotaxic template atlas provided by Ferris et al. (2014).

(Deffains and Bergman, 2015). SCIs exert their effects via the release of acetylcholine (ACh), which act on muscarinic receptors of striatal medium spiny neurons (MSNs). In control mice, HFS of the striatum inhibits the release of ACh from SCIs – promoting MSN calcium influx and a resultant inhibition of glutamate-mediated sensorimotor activation (Calabresi et al., 1992; Dang et al., 2012; Pisani et al., 2006; Wang et al., 2006; see also Aosaki et al., 1994). In vitro studies, however, have shown that WT mice have a reduction in the autonomous pace-making tone of SCIs in response to striatal HFS, whereas the tonic firing patterns of SCIs in Dyt1 KI mice remain elevated (i.e., LTD deficit: Dang et al., 2012; Maltese et al., 2014; Yokoi et al., 2015). This finding has been attributed to the disrupted binding affinity of D2 dopamine receptors in the indirect basal ganglia pathway (Balcioglu et al., 2007; Calabresi et al., 1992) and the resultant disinhibition of ACh release from SCIs (Dang et al., 2012; Martella et al., 2009; Napolitano et al., 2010; Pisani et al., 2006).

Given the above findings, the current study used ICA on the resting-state fMRI data to contrast functional connectivity within basal ganglia regions across Dyt1 KI and WT mice. Our findings demonstrate a significant increase in functional connectivity in the striatum and thalamus of Dyt1 KI mice, providing further evidence that impaired functional interaction among neurons within the basal ganglia circuit contributes to the pathophysiology underlying DYT1 dystonia. It is important to recognize, however, that mice genotyped for the heterozygous ΔE mutation are overtly asymptomatic for abnormal contorted postures as observed in heterozygous Tor1a KO mice (Liang et al., 2014; Pappas et al., 2015). Thus, the observations in this paper could be viewed as an endophenotype for the genetic underpinnings triggered by the ΔE mutation. An alternative viewpoint is that the observations could be compensatory for the underlying pathophysiology. A number of studies have shown that cortico-striatal synaptic efficacy (i.e., LTD) and impaired motor function are restored in Dyt1 KI (Dang et al., 2012; DeAndrade et al., 2016; Maltese et al., 2014) and KO (Liang et al., 2014; Pappas et al., 2015) mice following the administration of anticholinergic therapeutics. As such, future studies focused on elucidating restorative effects of anticholinergic medications on functional connectivity abnormalities will prove to be important in supporting the position that impaired basal ganglia connectivity manifests as a function of disease-specific pathogenesis.

To examine striatal FW and FA_T in Dyt1 KI and WT mice we analyzed the dMRI data using a novel bi-tensor diffusion analysis pipeline (Pasternak et al., 2009; Pasternak et al., 2012; see also Ofori et al., 2015a; Ofori et al., 2015b; Planetta et al., 2016). Using a bi-tensor model can be important because conventional single-tensor diffusion models do not account for extracellular FW within the voxel, which can bias diffusion measures such as fractional anisotropy (FA) (Metzler-Baddeley et al., 2012). We found that FW values in the dorsal striatum were significantly increased in Dyt1 KI mice compared to their WT control counterparts. Further, our correlation analysis yielded a significant negative correlation between striatal FW and functional connectivity in the primary motor cortex, and the anisiform and paramedian lobules of the cerebellum. This finding of altered striatal integrity supports prior work by Uluğ et al. (2011) who reported a significant reduction in FA in the dorsal striatum of Dyt1 KI mice. In the current study, we accounted for FW elevation within the voxel and did not find between-group differences in FA_T. Thus, it appears that it is the FW metric that is driving the FA changes in the striatum in Dyt1 KI mice previously found using a single-tensor model (Uluğ et al., 2011). As well, Pappas et al. (2015) found that the selective KO of TA within forebrain cholinergic and GABAergic progenitors caused a 40–50% reduction in the number of SCIs in the dorsal striatum of Dyt1 mice. This represents a salient finding as abnormal striatal pathology

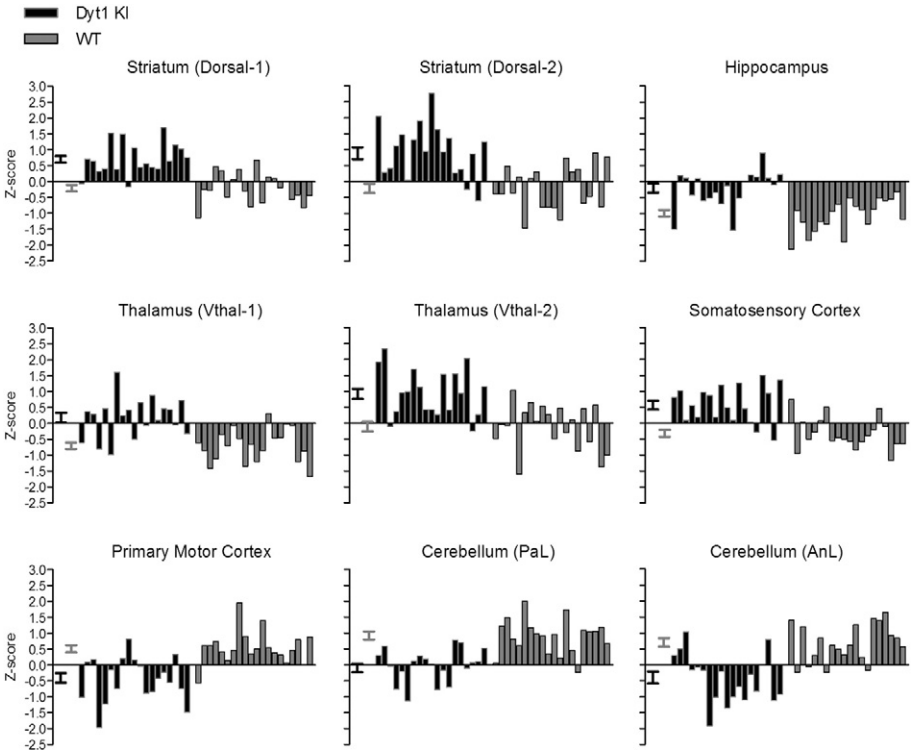

Fig. 5. Between-groups functional connectivity z-score plots. Comparison of subject-by-subject mean z-score values from components where significant between-group differences were detected across Dyt1 KI (black bars) and WT (grey bars) mice. Black and grey error bars represent ±1 SE centered on the mean z-score for Dyt1 KI and WT mice, respectively. Dorsal-1, dorsal striatum component 1 (Fig. 2A); Dorsal-2, dorsal striatum component 2 (Fig. 2B); Vthal-1, ventral thalamic area component 1 (Fig. 3B); Vthal-2, ventral thalamic area component 2 (Fig. 3A); PaL, paramedian lobule of cerebellum; AnL, anisiform lobule of cerebellum.

in Dyt1 KO mice produces a behavioral phenotype consistent with abnormal contracture commonly expressed in manifesting DYT1 gene carriers (see also Liang et al., 2014; Weisheit and Dauer, 2015). Our results add to this work insomuch as it demonstrates that microstructural abnormalities in the striatum relate to network level impairments in cortical and cerebellar functional connectivity.

Table 1
Summary of support vector machine classification model.

Component cluster(s)	AUC	Prediction
STR (Dorsal-1)	1.0	100
STR (Dorsal-2)	0.63	46.7
STR (Dorsal-1); (Dorsal-2)	0.84	73.3
CBX (PaL)	0.8	66.7
CBX (AnL)	0.93	80
CBX (PaL); CBX (AnL)	0.96	80
STR (Dorsal-1); CBX (PaL)	0.95	86.7
STR (Dorsal-1), (Dorsal-2); CBX (PaL), (AnL)	0.86	66.7
PSC	0.86	73.3
PSC (Dorsal-1)	0.96	80
PSC; STR (Dorsal-1), (Dorsal-2)	0.95	86.7
PSC; CBX (PaL), (AnL)	1	86.7
PSC; STR (Dorsal-1), (Dorsal-2); CBX (PaL), (AnL)	0.95	80
HIP	1	73.3
THA (Vthal-1)	0.89	73.3
THA (Vthal-2)	0.88	80
THA (Vthal-1), (Vthal-2)	0.96	80
HIP; THA (Vthal-1), (Vthal-2)	0.98	93.3
STR (Dorsal-1), (Dorsal-2); CBX (PaL), (AnL), THA (Vthal-1), (Vthal-2)	0.98	93.3
PMC	0.95	93.3
PMC; STR (Dorsal-1), (Dorsal-2)	1	93.3
PMC; CBX (PaL), (AnL)	0.98	93.3
PMC; THA (Vthal-1), (Vthal-2)	0.96	80
PMC; THA (Vthal-1), (Vthal-2); HIP	0.98	80
STR (Dorsal-1); HIP; CBX (AnL); PSC; PMC; THA (Vthal-1)	1	93.3

The results of the support vector machine cross-validation analysis based on mean functional connectivity z-score measures in a training cohort of 12 DYT1 KI and 12 WT; and evaluated in a testing cohort of 15 mice (seven Dyt1 KI and eight WT). AUC, training cohort area under the curve; CBX, cerebellar cortex; HIP, hippocampus; PMC, primary motor cortex; Prediction, testing cohort classification accuracy; PSC, primary somatosensory cortex; STR, striatum; THA, thalamus.

4.2. Sensorimotor cortical connectivity in Dyt1 KI mice

Dyt1 KI mice showed decreased functional connectivity in the primary motor cortex and increased functional connectivity in the somatosensory cortex compared to WT controls. These findings extend prior work employing $H_2^{15}O$-PET showing abnormal network level activation patterns of the sensorimotor cortex in human DYT1 dystonia patients (Carbon et al., 2010). As well, previous human studies contend that increased EMG activation patterns and muscular co-contraction in dystonia (Berardelli et al., 1996; Berardelli et al., 1998) is attributed, in part, to impaired motor cortical surround inhibition (SI: Beck and Hallett, 2011; Hallett, 2011; Mink, 1996; Sohn and Hallett, 2004a; Sohn and Hallett, 2004b). SI is characterized by a transient, top-down inhibition (i.e., response suppression) of motor cortical excitability, which serves to facilitate selection between different populations of motor neurons competing for a common movement threshold (Mink, 1996; Sohn and Hallett, 2004b). The most frequently examined SI paradigm involves using transcranial magnetic stimulation (TMS) and cortical motor evoked potentials (MEPs) prior to – and during – the initiation of goal-directed (i.e., voluntary) movement. For example, Sohn and Hallett (2004a) delivered self-triggered motor cortical TMS at various intervals following initial EMG activation in the flexor digitorum superficialis muscle during a self-paced finger flexion task. The authors reported that MEPs related to several finger flexion muscles were significantly increased in focal hand dystonia patients compared to normal healthy controls (see also Ridding et al., 1995).

In terms of somatosensory-related increase in functional connectivity, our data suggest that the functional organization of somatosensory cortical neurons are enhanced in Dyt1 KI mice when integrating sensory feedback related to amplified cortical motor drive via the basal ganglia.

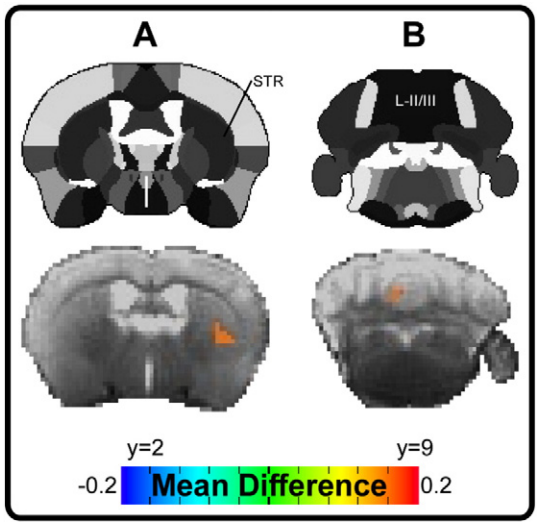

Fig. 6. Between-group comparisons of striatal and cerebellar free-water. Color bars represent the mean difference in free-water values for between-group post-hoc comparisons (i.e., Dyt1 KI versus WT). Results are thresholded at $P < 0.005$ at the voxel level and FWER corrected at $P < 0.05$. Positive values, represented by warm (red) colors, denote a significant increase in free-water in Dyt1 KI mice compared to WT mice in (A) dorsal striatum, STR, and (B) lobule II/III of the cerebellum, L-II/III. Spatial color maps are superimposed over the b0 image of a single subject. Stereotaxic template atlas provided by Ferris et al. (2014).

As described above, previous work has reported that Dyt1 KI mice elicit impaired inhibitory modulation of cortical evoked potentials via striatal HFS in vitro (Dang et al., 2012). Moreover, abnormal sensorimotor evoked functional connectivity may account for recent evidence that the Dyt1 KI mouse model elicits sustained EMG activity and intermittent co-contractions of the biceps and rectus femori muscles (DeAndrade et al., 2016). These findings are in line with previous human studies that have reported increased volumetric grey-matter changes and amplified somatosensory activation in accounting for the overflow of conflicting cortical motor commands (i.e., SI) in patients with writer's cramp, orofacial dystonia, and focal hand dystonia (Dresel et al., 2006; Garraux et al., 2004; Lerner et al., 2004). Simonyan and Ludlow (2010) showed that symptomatic voice production in focal spasmodic dysphonia patients is associated with increased motor and somatosensory related activity; and similar abnormalities in sensorimotor evoked activity have been reported in other task-specific focal dystonias (Haslinger et al., 2010; Pujol et al., 2000). In addition, Nelson et al. (2009) showed overlapping activation patterns in the somatotopic representation of the first three hand digits in patients with task-specific writer's cramp.

4.3. Cerebellar structure-function relationship in Dyt1 KI mice

Although dystonia is primarily considered a basal ganglia circuit disorder, recent literature has emphasized a clear role of the cerebellum in motor dysfunction. For example, previous work has shown that surgical removal of the cerebellum can eradicate the paroxysmal dystonic effects of toxic vectors (i.e., 6-hydroxydopamine, quinolinic acid) that induce widespread striatal degeneration (Neychev et al., 2008; see also Campbell et al., 1999; Chen et al., 2014). Our results showed that Dyt1 KI mice were associated with decreased functional connectivity within two regions of the cerebellar cortex: the anisiform and paramedian lobules. Notably, functional connectivity patterns in these regions yielded a strong AUC and moderate-to-high classification accuracy (0.8/66.7 and 0.93/80.0 for paramedian and anisiform lobules, respectively). These findings are consistent with previous PET work showing abnormalities

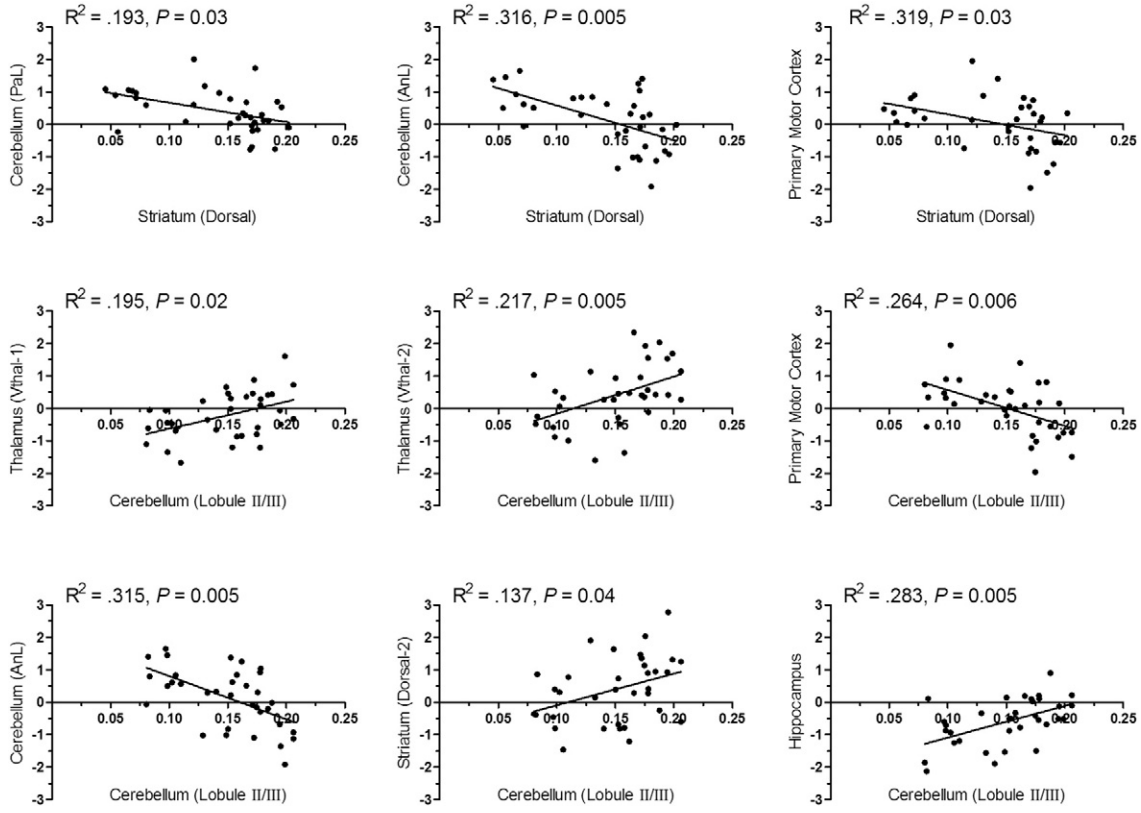

Fig. 7. Pearson's correlation coefficients relating subject-specific mean free-water values in the striatum and cerebellum (*x*-axis) with mean functional connectivity z-scores (*y*-axis). We employed a false discovery rate (FDR) at 0.05 to correct for multiple comparisons. Free-water in the striatum was negatively correlated with functional connectivity in the paramedian (PaL) and anisiform (AnL) lobules of the cerebellum, and the primary motor cortex. Free-water in the cerebellum was positively correlated with functional connectivity in the ventral thalamic areas (Vthal-1, Vthal-2), striatum (Dorsal-2), and hippocampus; and negatively correlated with functional connectivity in the primary motor cortex and AnL.

in regional cerebellar metabolism in both manifesting and non-manifesting DYT1 gene carriers (Carbon et al., 2004; Carbon et al., 2008a; Eidelberg et al., 1998); and decreased alteration of amplitude of low-frequency fluctuations (Biswal et al., 1995) in the cerebellum in patients with benign essential blepharospasm (Zhou et al., 2013). Abnormal regional glucose metabolism and utilization has also been demonstrated using in vivo PET in the cerebellar vermis of Dyt1 KI and KO mice (Uluğ et al., 2011; Vo et al., 2015a) and the Purkinje cell layer of the cerebellum in hMT mice (Zhao et al., 2011). These findings have been attributed to decreased inhibitory input to the vermis via cerebellar Purkinje cells (Vo et al., 2015a). Indeed, previous work has shown that Dyt1 KI and Purkinje-cell specific Dyt1 KO pathology is characterized by microstructural abnormalities and reduced quantity of cerebellar Purkinje cell dendrites and spines (Zhang et al., 2011). It is possible that in the current study, morphological changes to Purkinje cell dendrites in the anisiform and paramedian lobules impair the functional connectivity of neurons within these regions.

Interestingly, in the same line of Dyt1 KI mice (Dang et al., 2005; Zhang et al., 2011), FW values were increased compared to WT controls in lobule II/III of the cerebellum – which contains a high concentration of cerebellar Purkinje neurons (Ozol et al., 1999). These findings extend prior work that used single-tensor analyses of dMRI data and reported significant FA reductions and microstructural changes within cerebellar regions in human DYT1 dystonia patients (Argyelan et al., 2009; Carbon et al., 2008b; Vo et al., 2015b). Only one previous study has examined structural changes in Dyt1 KI mice using dMRI. In particular, Uluğ et al. (2011) employed a single-tensor tractography analysis to determine the structural integrity of the cerebellothalamocortical tract and reported significant FA reductions within the cerebellum. After correcting for FW contamination, the results from the current study did not reveal between-group differences in FA_T values. Thus, our results provide new evidence that extracellular FW may serve as a sensitive measure of microstructural abnormalities of cerebellar and basal ganglia regions in a mouse model of DYT1 dystonia. Further, the correlation analysis establishes a clear relationship between cerebellar microstructural integrity and functional connectivity patterns across the primary motor cortex, striatum, thalamus, and cerebellar cortex (anisiform lobule).

It remains unclear whether functional connectivity patterns revealed in the cerebellar cortex are related to the respective increase and decrease in functional connectivity in the somatosensory-basal ganglia circuit and primary motor cortex. Indeed, anatomical tracing and electrophysiological studies have shown that the sensorimotor cortex, basal ganglia and cerebellum comprise a major parallel multi-synaptic (i.e., afferent and efferent) cortical pathway – and that cerebellar Purkinje cell output mediates the excitability of striatal neurons via disynaptic cerebello-thalamo projections (Bostan and Strick, 2010; Chen et al., 2014; Hoshi et al., 2005; Middleton, 2000). For example, Chen et al. (2014) demonstrated that stimulation of cerebellar dentate nucleus and intralaminar thalamic nuclei in awake mice produced a proportional, short-latency increase in the firing rate of striatal MSNs. The current findings of abnormalities in fMRI and dMRI measures across the cortex, basal ganglia and cerebellum further contribute to the hypothesis that DYT1 dystonia likely results from a network level change across structures within these regions.

There are several limitations to note in this study. In particular, it remains to be determined whether the subtle motor impairments that exist in the Dyt1 KI mouse model (Dang et al., 2005; Yokoi et al., 2015) can be regarded as a reliable experimental representation of motor impairments in human DYT1 patients. The Dyt1 KI mouse model used in the current paradigm represents a genetically derived experimental corollary of both manifesting and non-manifesting human DYT1 gene carriers. Although Dyt1 KI mice demonstrate hyperactive behavior and subtle motor impairments, they remain resistant to the expression of an overt contracture-like dystonic phenotype observed in other Tor1a KO mouse models (Liang et al., 2014; Pappas et al., 2015). Notably, however, recent intramuscular EMG evidence has shown that compared to WT mice, Dyt1 KI mice are characterized by an increase in sustained contractions and intermittent co-contractile properties of the biceps and rectus femori muscles (DeAndrade et al., 2016). Furthermore, such antagonistic electrical potential of opposing muscle groups is alleviated via the administration of anti-cholinergic therapeutics (DeAndrade et al., 2016). Second, in the current study mice were induced to resting-state using isoflurane anesthesia at 2% concentration and maintained in an unconscious state for the duration of the imaging protocol at concentrations between 1 and 1.5%. Previous work has shown that isoflurane in rodents at high doses (i.e., >1.8%) interferes with functional connectivity patterns and produces less defined network level spatial segmentation (Liu et al., 2013), whereas isoflurane at lower doses (i.e., <1.5%) preserves resting-state functional connectivity patterns and anatomical decomposition of resting-state sub-networks (Ferron et al., 2009; Liu et al., 2013). Given these findings, we do not anticipate that any confounding effects of isoflurane anesthesia contributed to between-group differences in functional connectivity patterns across cortical and subcortical brain regions in the current study.

In summary, the current study provides the first in vivo MRI-based evidence that the removal of a single glutamic acid residue in the carboxyl terminus of the Tor1a protein engenders impaired network level functional connectivity and microstructural abnormalities across cortical and subcortical brain regions. The functional connectivity patterns were robust in machine learning algorithms for training and test datasets. Further, the microstructural elevation of FW in the striatum and cerebellum correlated with the patterns of functional connectivity. Future studies that use these techniques in other animal models of dystonia that show a robust phenotype (Liang et al., 2014; Pappas et al., 2015) will prove important in furthering our understanding of connectivity abnormalities and pathophysiology of dystonia.

Conflict of interest

The authors report no existing conflict of interest.

Acknowledgements

Mouse template atlas provided by Ekam Solutions, LLC (Craig F. Ferris and Praveen Kulkarni). Funding: This research was supported by grants from Tyler's Hope for a Dystonia Cure, Inc., the National Institutes of Health (grant numbers R01 NS075012, R01 NS058487, R01 NS082244, T32 NS082168), and a University of Florida McKnight Brain Institute pilot imaging grant. Data collection was performed in the McKnight Brain Institute at the National High Magnetic Field Laboratory's AMRIS Facility, which is supported by National Science Foundation Cooperative Agreement No. DMR-1157490 and the State of Florida. This work was supported in part by a National Institutes of Health award (S10RR025671) for MRI/S instrumentation.

References

Albanese, A., Bhatia, K., Bressman, S.B., Delong, M.R., Fahn, S., Fung, V.S., Hallett, M., Jankovic, J., Jinnah, H.A., Klein, C., Lang, A.E., Mink, J.W., Teller, J.K., 2013. Phenomenology and classification of dystonia: a consensus update. Mov. Disord. 28, 863–873.

Aosaki, T., Tsubokawa, H., Ishida, A., Watanabe, K., Graybiel, A.M., Kimura, M., 1994. Responses of tonically active neurons in the primate's striatum undergo systematic changes during behavioral sensorimotor conditioning. J. Neurosci. 14, 3969–3984.

Argyelan, M., Carbon, M., Niethammer, M., Uluğ, A.M., Voss, H.U., Bressman, S.B., Dhawan, V., Eidelberg, D., 2009. Cerebellothalamocortical connectivity regulates penetrance in dystonia. J. Neurosci. 29, 9740–9747.

Balcioglu, A., Kim, M.O., Sharma, N., Cha, J.H., Breakefield, X.O., Standaert, D.G., 2007. Dopamine release is impaired in a mouse model of DYT1 dystonia. J. Neurochem. 102, 783–788.

Beck, S., Hallett, M., 2011. Surround inhibition in the motor system. Exp. Brain Res. 210, 165–172.

Berardelli, A., Hallett, M., Rothwell, J.C., Agostino, R., Manfredi, M., Thompson, P.D., Marsden, C.D., 1996. Single-joint rapid arm movements in normal subjects and in patients with motor disorders. Brain 119 (Pt 2), 661–674.

Berardelli, A., Rothwell, J.C., Hallett, M., Thompson, P.D., Manfredi, M., Marsden, C.D., 1998. The pathophysiology of primary dystonia. Brain 121 (Pt 7), 1195–1212.
Biswal, B., Yetkin, F.Z., Haughton, V.M., Hyde, J.S., 1995. Functional connectivity in the motor cortex of resting human brain using echo-planar MRI. Magn. Reson. Med. 34, 537–541.
Bostan, A.C., Strick, P.L., 2010. The cerebellum and basal ganglia are interconnected. Neuropsychol. Rev. 20, 261–270.
Breakefield, X.O., Blood, A.J., Li, Y., Hallett, M., Hanson, P.I., Standaert, D.G., 2008. The pathophysiological basis of dystonias. Nat. Rev. Neurosci. 9, 222–234.
Calabresi, P., Maj, R., Pisani, A., Mercuri, N.B., Bernardi, G., 1992. Long-term synaptic depression in the striatum: physiological and pharmacological characterization. J. Neurosci. 12, 4224–4233.
Calhoun, V.D., Adali, T., 2012. Multisubject independent component analysis of fMRI: a decade of intrinsic networks, default mode, and neurodiagnostic discovery. IEEE Rev. Biomed. Eng. 5, 60–73.
Calhoun, V.D., Adali, T., Pearlson, G.D., Pekar, J.J., 2001a. A method for making group inferences from functional MRI data using independent component analysis. Hum. Brain Mapp. 14, 140–151.
Calhoun, V.D., Adali, T., Pearlson, G.D., Pekar, J.J., 2001b. Spatial and temporal independent component analysis of functional MRI data containing a pair of task-related waveforms. Hum. Brain Mapp. 13, 43–53.
Campbell, D.B., North, J.B., Hess, E.J., 1999. Tottering mouse motor dysfunction is abolished on the Purkinje cell degeneration (pcd) mutant background. Exp. Neurol. 160, 268–278.
Carbon, M., Su, S., Dhawan, V., Raymond, D., Bressman, S., Eidelberg, D., 2004. Regional metabolism in primary torsion dystonia: effects of penetrance and genotype. Neurology 62, 1384–1390.
Carbon, M., Ghilardi, M.F., Argyelan, M., Dhawan, V., Bressman, S.B., Eidelberg, D., 2008a. Increased cerebellar activation during sequence learning in DYT1 carriers: an equiperformance study. Brain 131, 146–154.
Carbon, M., Kingsley, P.B., Tang, C., Bressman, S., Eidelberg, D., 2008b. Microstructural white matter changes in primary torsion dystonia. Mov. Disord. 23, 234–239.
Carbon, M., Argyelan, M., Habeck, C., Ghilardi, M.F., Fitzpatrick, T., Dhawan, V., Pourfar, M., Bressman, S.B., Eidelberg, D., 2010. Increased sensorimotor network activity in DYT1 dystonia: a functional imaging study. Brain 133, 690–700.
Centonze, D., Picconi, B., Gubellini, P., Bernardi, G., Calabresi, P., 2001. Dopaminergic control of synaptic plasticity in the dorsal striatum. Eur. J. Neurosci. 13, 1071–1077.
Chang, C.-C., Lin, C.-J., 2011. LIBSVM: a library for support vector machines. ACM Trans. Intell. Syst. Technol. 2, 27.
Chen, C.H., Fremont, R., Arteaga-Bracho, E.E., Khodakhah, K., 2014. Short latency cerebellar modulation of the basal ganglia. Nat. Neurosci. 17, 1767–1775.
Cox, R.W., 1996. AFNI: software for analysis and visualization of functional magnetic resonance neuroimages. Comput. Biomed. Res. 29, 162–173.
Dang, M.T., Yokoi, F., McNaught, K.S., Jengelley, T.A., Jackson, T., Li, J., Li, Y., 2005. Generation and characterization of Dyt1 DeltaGAG knock-in mouse as a model for early-onset dystonia. Exp. Neurol. 196, 452–463.
Dang, M.T., Yokoi, F., Cheetham, C.C., Lu, J., Vo, V., Lovinger, D.M., Li, Y., 2012. An anticholinergic reverses motor control and corticostriatal LTD deficits in Dyt1 ΔGAG knock-in mice. Behav. Brain Res. 226, 465–472.
DeAndrade, M.P., Trongnetrpunya, A., Yokoi, F., Cheetham, C.C., Peng, N., Wyss, J.M., Ding, M., Li, Y., 2016. Electromyographic evidence in support of a knock-in mouse model of DYT1 Dystonia. Mov. Disord.
Deffains, M., Bergman, H., 2015. Striatal cholinergic interneurons and cortico-striatal synaptic plasticity in health and disease. Mov. Disord. 30, 1014–1025.
Dresel, C., Haslinger, B., Castrop, F., Wohlschlaeger, A.M., Ceballos-Baumann, A.O., 2006. Silent event-related fMRI reveals deficient motor and enhanced somatosensory activation in orofacial dystonia. Brain 129, 36–46.
Eidelberg, D., Moeller, J.R., Antonini, A., Kazumata, K., Nakamura, T., Dhawan, V., Spetsieris, P., deLeon, D., Bressman, S.B., Fahn, S., 1998. Functional brain networks in DYT1 dystonia. Ann. Neurol. 44, 303–312.
Fahn, S., 1988. Concept and classification of dystonia. Adv. Neurol. 50, 1–8.
Ferris, C.F., Kulkami, P., Toddes, S., Yee, J., Kenkel, W., Nedelman, M., 2014. Studies on the Q175 knock-in model of Huntington's disease using functional imaging in awake mice: evidence of olfactory dysfunction. Front. Neurol. 5 (94).
Ferron, J.F., Kroeger, D., Chever, O., Amzica, F., 2009. Cortical inhibition during burst suppression induced with isoflurane anesthesia. J. Neurosci. 29, 9850–9860.
Garraux, G., Bauer, A., Hanakawa, T., Wu, T., Kansaku, K., Hallett, M., 2004. Changes in brain anatomy in focal hand dystonia. Ann. Neurol. 55, 736–739.
Goodchild, R.E., Dauer, W.T., 2005. The AAA+ protein torsinA interacts with a conserved domain present in LAP1 and a novel ER protein. J. Cell Biol. 168, 855–862.
Goodchild, R.E., Kim, C.E., Dauer, W.T., 2005. Loss of the dystonia-associated protein torsinA selectively disrupts the neuronal nuclear envelope. Neuron 48, 923–932.
Goodchild, R.E., Buchwalter, A.L., Naismith, T.V., Holbrook, K., Billion, K., Dauer, W.T., Liang, C.C., Dear, M.L., Hanson, P.I., 2015. Access of torsinA to the inner nuclear membrane is activity dependent and regulated in the endoplasmic reticulum. J. Cell Sci. 128, 2854–2865.
Hallett, M., 2011. Neurophysiology of dystonia: the role of inhibition. Neurobiol. Dis. 42, 177–184.
Haslinger, B., Altenmüller, E., Castrop, F., Zimmer, C., Dresel, C., 2010. Sensorimotor overactivity as a pathophysiologic trait of embouchure dystonia. Neurology 74, 1790–1797.
Hewett, J.W., Tannous, B., Niland, B.P., Nery, F.C., Zeng, J., Li, Y., Breakefield, X.O., 2007. Mutant torsinA interferes with protein processing through the secretory pathway in DYT1 dystonia cells. Proc. Natl. Acad. Sci. U. S. A. 104, 7271–7276.
Hoshi, E., Tremblay, L., Féger, J., Carras, P.L., Strick, P.L., 2005. The cerebellum communicates with the basal ganglia. Nat. Neurosci. 8, 1491–1493.
Jonckers, E., Van Audekerke, J., De Visscher, G., Van der Linden, A., Verhoye, M., 2011. Functional connectivity fMRI of the rodent brain: comparison of functional connectivity networks in rat and mouse. PLoS One 6, e18876.
Lerner, A., Shill, H., Hanakawa, T., Bushara, K., Goldfine, A., Hallett, M., 2004. Regional cerebral blood flow correlates of the severity of writer's cramp symptoms. NeuroImage 21, 904–913.
Liang, C.C., Tanabe, L.M., Jou, S., Chi, F., Dauer, W.T., 2014. TorsinA hypofunction causes abnormal twisting movements and sensorimotor circuit neurodegeneration. J. Clin. Invest. 124, 3080–3092.
Liu, X., Zhu, X.H., Zhang, Y., Chen, W., 2013. The change of functional connectivity specificity in rats under various anesthesia levels and its neural origin. Brain Topogr. 26, 363–377.
Maltese, M., Martella, G., Madeo, G., Fagiolo, I., Tassone, A., Ponterio, G., Sciamanna, G., Burbaud, P., Conn, P.J., Bonsi, P., Pisani, A., 2014. Anticholinergic drugs rescue synaptic plasticity in DYT1 dystonia: role of M1 muscarinic receptors. Mov. Disord. 29, 1655–1665.
Martella, G., Tassone, A., Sciamanna, G., Platania, P., Cuomo, D., Viscomi, M.T., Bonsi, P., Cacci, E., Biagioni, S., Usiello, A., Bernardi, G., Sharma, N., Standaert, D.G., Pisani, A., 2009. Impairment of bidirectional synaptic plasticity in the striatum of a mouse model of DYT1 dystonia: role of endogenous acetylcholine. Brain 132, 2336–2349.
McKeown, M.J., Makeig, S., Brown, G.G., Jung, T.P., Kindermann, S.S., Bell, A.J., Sejnowski, T.J., 1998. Analysis of fMRI data by blind separation into independent spatial components. Hum. Brain Mapp. 6, 160–188.
Mechling, A.E., Hübner, N.S., Lee, H.L., Hennig, J., von Elverfeldt, D., Harsan, L.A., 2014. Fine-grained mapping of mouse brain functional connectivity with resting-state fMRI. NeuroImage 96, 203–215.
Metzler-Baddeley, C., O'Sullivan, M.J., Bells, S., Pasternak, O., Jones, D.K., 2012. How and how not to correct for CSF-contamination in diffusion MRI. NeuroImage 59, 1394–1403.
Middleton, F., 2000. Basal ganglia and cerebellar loops: motor and cognitive circuits. Brain Res. Rev. 31, 236–250.
Mink, J.W., 1996. The basal ganglia: focused selection and inhibition of competing motor programs. Prog. Neurobiol. 50, 381–425.
Napolitano, F., Pasqualetti, M., Usiello, A., Santini, E., Pacini, G., Sciamanna, G., Errico, F., Tassone, A., Di Dato, V., Martella, G., Cuomo, D., Fisone, G., Bernardi, G., Mandolesi, G., Mercuri, N.B., Standaert, D.G., Pisani, A., 2010. Dopamine D2 receptor dysfunction is rescued by adenosine A2A receptor antagonism in a model of DYT1 dystonia. Neurobiol. Dis. 38, 434–445.
Nelson, A.J., Blake, D.T., Chen, R., 2009. Digit-specific aberrations in the primary somatosensory cortex in Writer's cramp. Ann. Neurol. 66, 146–154.
Neychev, V.K., Fan, X., Mitev, V.I., Hess, E.J., Jinnah, H.A., 2008. The basal ganglia and cerebellum interact in the expression of dystonic movement. Brain 131, 2499–2509.
Ofori, E., Pasternak, O., Planetta, P.J., Burciu, R., Snyder, A., Febo, M., Golde, T.E., Okun, M.S., Vaillancourt, D.E., 2015a. Increased free water in the substantia nigra of Parkinson's disease: a single-site and multi-site study. Neurobiol. Aging 36, 1097–1104.
Ofori, E., Pasternak, O., Planetta, P.J., Li, H., Burciu, R.G., Snyder, A.F., Lai, S., Okun, M.S., Vaillancourt, D.E., 2015b. Longitudinal changes in free-water within the substantia nigra of Parkinson's disease. Brain 138, 2322–2331.
Ozelius, L.J., Hewett, J.W., Page, C.E., Bressman, S.B., Kramer, P.L., Shalish, C., de Leon, D., Brin, M.F., Raymond, D., Corey, D.P., Fahn, S., Risch, N.J., Buckler, A.J., Gusella, J.F., Breakefield, X.O., 1997. The early-onset torsion dystonia gene (DYT1) encodes an ATP-binding protein. Nat. Genet. 17, 40–48.
Ozeluis, L.J., Lubarr, N., 1993. DYT1 early-onset primary dystonia. In: Pagon, R.A., et al. (Eds.), GeneReviews(®). University of Washington, Seattle, Seattle.
Ozol, K., Hayden, J.M., Oberdick, J., Hawkes, R., 1999. Transverse zones in the vermis of the mouse cerebellum. J. Comp. Neurol. 412, 95–111.
Pappas, S.S., Darr, K., Holley, S.M., Cepeda, C., Mabrouk, O.S., Wong, J.M., LeWitt, T.M., Paudel, R., Houlden, H., Kennedy, R.T., Levine, M.S., Dauer, W.T., 2015. Forebrain deletion of the dystonia protein torsinA causes dystonic-like movements and loss of striatal cholinergic neurons. Elife 4, e08352.
Pasternak, O., Sochen, N., Gur, Y., Intrator, N., Assaf, Y., 2009. Free water elimination and mapping from diffusion MRI. Magn. Reson. Med. 62, 717–730.
Pasternak, O., Westin, C.F., Bouix, S., Seidman, L.J., Goldstein, J.M., Woo, T.U., Petryshen, T.L., Mesholam-Gately, R.I., McCarley, R.W., Kikinis, R., Shenton, M.E., Kubicki, M., 2012. Excessive extracellular volume reveals a neurodegenerative pattern in schizophrenia onset. J. Neurosci. 32, 17365–17372.
Pisani, A., Martella, G., Tscherter, A., Bonsi, P., Sharma, N., Bernardi, G., Standaert, D.G., 2006. Altered responses to dopaminergic D2 receptor activation and N-type calcium currents in striatal cholinergic interneurons in a mouse model of DYT1 dystonia. Neurobiol. Dis. 24, 318–325.
Planetta, P.J., Ofori, E., Pasternak, O., Burciu, R.G., Shukla, P., DeSimone, J.C., Okun, M.S., McFarland, N.R., Vaillancourt, D.E., 2016. Free-water imaging in Parkinson's disease and atypical parkinsonism. Brain 139, 495–508.
Pujol, J., Roset-Llobet, J., Rosinés-Cubells, D., Deus, J., Narberhaus, B., Valls-Solé, J., Capdevila, A., Pascual-Leone, A., 2000. Brain cortical activation during guitar-induced hand dystonia studied by functional MRI. NeuroImage 12, 257–267.
Ridding, M.C., Sheean, G., Rothwell, J.C., Inzelberg, R., Kujirai, T., 1995. Changes in the balance between motor cortical excitation and inhibition in focal, task specific dystonia. J. Neurol. Neurosurg. Psychiatry 59, 493–498.
Simonyan, K., Ludlow, C.L., 2010. Abnormal activation of the primary somatosensory cortex in spasmodic dysphonia: an fMRI study. Cereb. Cortex 20, 2749–2759.
Sohn, Y.H., Hallett, M., 2004a. Disturbed surround inhibition in focal hand dystonia. Ann. Neurol. 56, 595–599.
Sohn, Y.H., Hallett, M., 2004b. Surround inhibition in human motor system. Exp. Brain Res. 158, 397–404.
Tanabe, L.M., Kim, C.E., Alagem, N., Dauer, W.T., 2009. Primary dystonia: molecules and mechanisms. Nat. Rev. Neurol. 5, 598–609.

Uluğ, A.M., Vo, A., Argyelan, M., Tanabe, L., Schiffer, W.K., Dewey, S., Dauer, W.T., Eidelberg, D., 2011. Cerebellothalamocortical pathway abnormalities in torsinA DYT1 knock-in mice. Proc. Natl. Acad. Sci. U. S. A. 108, 6638–6643.

van der Kamp, W., Berardelli, A., Rothwell, J.C., Thompson, P.D., Day, B.L., Marsden, C.D., 1989. Rapid elbow movements in patients with torsion dystonia. J. Neurol. Neurosurg. Psychiatry 52, 1043–1049.

Vo, A., Sako, W., Dewey, S.L., Eidelberg, D., Uluğ, A.M., 2015a. 18FDG-microPET and MR DTI findings in Tor1a+/- heterozygous knock-out mice. Neurobiol. Dis. 73, 399–406.

Vo, A., Sako, W., Niethammer, M., Carbon, M., Bressman, S.B., Uluğ, A.M., Eidelberg, D., 2015b. Thalamocortical connectivity correlates with phenotypic variability in dystonia. Cereb. Cortex 25, 3086–3094.

Wang, Z., Kai, L., Day, M., Ronesi, J., Yin, H.H., Ding, J., Tkatch, T., Lovinger, D.M., Surmeier, D.J., 2006. Dopaminergic control of corticostriatal long-term synaptic depression in medium spiny neurons is mediated by cholinergic interneurons. Neuron 50, 443–452.

Weisheit, C.E., Dauer, W.T., 2015. A novel conditional knock-in approach defines molecular and circuit effects of the DYT1 dystonia mutation. Hum. Mol. Genet. 24, 6459–6472.

Yokoi, F., Dang, M.T., Liu, J., Gandre, J.R., Kwon, K., Yuen, R., Li, Y., 2015. Decreased dopamine receptor 1 activity and impaired motor-skill transfer in Dyt1 ΔGAG heterozygous knock-in mice. Behav. Brain Res. 279, 202–210.

Zhang, L., Yokoi, F., Jin, Y.H., DeAndrade, M.P., Hashimoto, K., Standaert, D.G., Li, Y., 2011. Altered dendritic morphology of Purkinje cells in Dyt1 ΔGAG knock-in and purkinje cell-specific Dyt1 conditional knockout mice. PLoS One 6, e18357.

Zhao, Y., Sharma, N., LeDoux, M.S., 2011. The DYT1 carrier state increases energy demand in the olivocerebellar network. Neuroscience 177, 183–194.

Zhou, B., Wang, J., Huang, Y., Yang, Y., Gong, Q., Zhou, D., 2013. A resting state functional magnetic resonance imaging study of patients with benign essential blepharospasm. J. Neuroophthalmol. 33, 235–240.